



Measurement of the  $t\bar{t}$  Production Cross Section  
at  $\sqrt{s} = 1.96$  TeV in Dilepton Final States using  $370 \text{ pb}^{-1}$  of DØ Data

*Results for Summer 2005 Conferences*

The DØ Collaboration  
(Dated: July 1, 2005)

We present a measurement of the top quark pair ( $t\bar{t}$ ) production cross section in  $p\bar{p}$  collisions at  $\sqrt{s} = 1.96$  TeV using events with  $ee$ ,  $e\mu$  or  $\mu\mu$  final states. This analysis utilizes an integrated luminosity of approximately  $370 \text{ pb}^{-1}$  collected with the DØ detector at the Fermilab Tevatron Collider. The cross-sections measured in the three channels separately are:

$$\begin{aligned} ee &: \quad \sigma_{t\bar{t}} = 7.9_{-3.8}^{+5.2} \text{ (stat)} \quad {}_{-1.0}^{+1.3} \text{ (syst)} \pm 0.5 \text{ (lumi) pb} \\ e\mu &: \quad \sigma_{t\bar{t}} = 10.2_{-2.6}^{+3.1} \text{ (stat)} \quad {}_{-1.3}^{+1.6} \text{ (syst)} \pm 0.7 \text{ (lumi) pb} \\ \mu\mu &: \quad \sigma_{t\bar{t}} = 1.8_{-3.0}^{+4.8} \text{ (stat)} \quad {}_{-1.2}^{+1.0} \text{ (syst)} \pm 0.1 \text{ (lumi) pb.} \end{aligned}$$

The combined cross section is:

$$\text{dilepton} : \quad \sigma_{t\bar{t}} = 8.6_{-2.0}^{+2.3} \text{ (stat)} \quad {}_{-1.0}^{+1.2} \text{ (syst)} \pm 0.6 \text{ (lumi) pb.}$$

## I. INTRODUCTION.

The top quark is the heaviest fermion and its mass could allow its decay into exotic particles, e.g. a charged Higgs boson [1]. The inclusive top pair ( $t\bar{t}$ ) production cross section ( $\sigma_{t\bar{t}}$ ) can be computed from individual  $t\bar{t}$  decay channels and their predicted standard model branching ratios. Exotic top decays would lead to different values of the inclusive top pair production cross section in the different channels. It is therefore important to precisely measure  $\sigma_{t\bar{t}}$  in all channels and compare it with the standard model prediction. Within the standard model each top quark of a  $t\bar{t}$  pair is expected to decay approximately 99.8% of the time to a  $W$  boson and a  $b$  quark [2]. Dilepton final states arise when both  $W$  bosons decay leptonically and occur along with two energetic jets resulting from the hadronization of the  $b$  quarks and with missing transverse energy ( $\cancel{E}_T$ ) from the high transverse momentum ( $p_T$ ) neutrinos.

The  $t\bar{t}$  production cross section in  $p\bar{p}$  collisions has been recently measured in dilepton final states using the datasets provided by the run II of the Tevatron [3]. In the present paper we update the  $D\bar{O}$  measurement using data taken in the period between April 2002 and August 2004, or 384, 368 and 363  $\text{pb}^{-1}$  in the  $e^+e^-$ ,  $e^\pm\mu^\mp$ , and  $\mu^+\mu^-$  channels, respectively. The electrons and muons may originate either directly from a  $W$  boson or indirectly from a  $W \rightarrow \tau\nu$  decay. The corresponding  $t\bar{t}$  branching fractions ( $B$ ) are 1.58%, 3.16%, and 1.57% [2] for the  $e^+e^-$ ,  $e^\pm\mu^\mp$ , and  $\mu^+\mu^-$  channels, respectively.

## II. LEPTON AND JET IDENTIFICATION

The  $D\bar{O}$  detector has a silicon microstrip tracker and a central fiber tracker located within a 2 T superconducting solenoidal magnet [4]. The surrounding liquid-argon/uranium calorimeter has a central cryostat covering pseudo-rapidities  $|\eta|$  up to 1.1 [5], and two end cryostats extending coverage to  $|\eta| \approx 4$  [6]. A muon system [7] resides beyond the calorimetry, and consists of a layer of tracking detectors and scintillation trigger counters before 1.8 T toroids, followed by two similar layers after the toroids. Luminosity is measured using plastic scintillator arrays located in front of the end cryostats.

Electrons are identified as clusters of calorimeter cells in a cone of size  $\Delta\mathcal{R} \equiv \sqrt{(\Delta\phi)^2 + (\Delta\eta)^2} = 0.4$ . Electron candidates are required to have a large fraction of their energy deposited in the electromagnetic layers of the calorimeter. The clusters are required to be isolated from hadronic energy, to have a matching charged track in the central tracking system and to have a shower shape consistent with that of an electron. Before the shower shape requirement electron candidates are referred to as “loose electrons”. We use both central ( $|\eta| < 1.1$ ) and forward ( $1.5 < |\eta| < 2.5$ ) electron candidates. In the  $e^+e^-$  channel we also require the electrons to be selected by a likelihood discriminant that combines information both from the central tracking system and the calorimeter in order to select isolated prompt electrons. Such electrons are referred to as “tight electrons”. In the  $e^\pm\mu^\mp$  channel we use a different approach. Instead of selecting electrons with a high value of the electron discriminant, we use the observed shape of the discriminant distribution in data to fit the fraction of events with one electron arising from instrumental background.

Muons are comprised of a track segment in the inner layer of the muon system, matching a segment formed from hits in the outer two muon layers of the muon system. A track in the central tracking system must also match the muon identified in the muon system, and the overall track  $\chi^2$  must be smaller than 4. To reject cosmic muons we apply cuts on the time of arrival of the muon tracks at the different layers of scintillators in the muon system. Muons supposedly originating from  $W$  or  $Z$  decays are identified using two isolation criteria: *i*) the energy deposited in the calorimeter in a hollow cone around the muon is smaller than 12% of the energy of the muon itself (this fraction is referred to as “calorimeter isolation”), *ii*) the scalar sum of the momenta of the charged tracks surrounding the muon track in the central tracking system is smaller than 12% of the muon track (this fraction is referred to as “tracker isolation”). To select prompt muons we also require that the significance of the distance of closest approach of the muon track with respect to the primary vertex ( $|dca|/\sigma_{dca}$ ) is smaller than 3. We refer to these muons as “tight” and we also consider for instrumental background calculations a second category of “loose muons” for which the tracker and calorimeter isolation are released.

Jets are reconstructed with a fixed cone of radius  $\Delta\mathcal{R} = 0.5$  [8] and must be confirmed by the independent calorimeter trigger readout. Jet energy calibration is applied to the jets [9]. The  $\cancel{E}_T$  is equal in magnitude and opposite in direction to the vector sum of the transverse energies in all calorimeter cells for which the energy is significantly above the noise. The transverse momenta of electrons and isolated muons are taken into account in  $\cancel{E}_T$  as well as the jet energy calibration.

### III. EVENT SELECTIONS

We select events with at least two jets with  $p_T^j > 20$  GeV and  $|y| < 2.5$  [5] and two charged leptons  $\ell$  with  $p_T^\ell > 15$  GeV. Muons are accepted in the region  $|\eta| < 2.0$ , while electrons must be within  $|\eta| < 1.1$  or  $1.5 < |\eta| < 2.5$ . The two leptons are required to be of opposite charge in all three channels. The large missing transverse energy due to the neutrinos in the  $t\bar{t}$  events is a powerful discriminant against background processes without high  $p_T$  neutrinos such as  $Z/\gamma^* \rightarrow \ell\bar{\ell}$ , where the  $\ell$  is either an electron or a muon. In the  $e^+e^-$  channel, we veto events with dielectron invariant mass  $80 \leq M_{ee} \leq 100$  GeV and require  $\cancel{E}_T > 35$  GeV ( $\cancel{E}_T > 40$  GeV) for  $M_{ee} > 100$  GeV ( $M_{ee} < 80$  GeV). In the  $e^\pm\mu^\mp$  channel we do not apply any cut on the  $\cancel{E}_T$ , while in the  $\mu^+\mu^-$  channel, we accept events with  $\cancel{E}_T > 35$  GeV. The  $\cancel{E}_T$  cut is tightened at low and high values of azimuthal distance  $\Delta\phi(\cancel{E}_T, \mu_1)$  between the leading  $p_T$  muon  $\mu_1$  and the direction of the  $\cancel{E}_T$ . Events with  $\Delta\phi(\cancel{E}_T, \mu_1) > 175^\circ$  are removed. The distribution of  $\Delta\phi(\cancel{E}_T, \mu_1)$  is shown in Fig. 1 in data and Monte Carlo in events with two opposite sign muons and with at least one jets.

The final selection in the  $e^\pm\mu^\mp$  channel requires  $H_T^\ell = p_T^{\ell_1} + \Sigma(p_T^j) > 122$  GeV, where  $p_T^{\ell_1}$  denotes the  $p_T$  of the leading lepton. This cut effectively rejects the largest backgrounds for this final state which arise from  $Z/\gamma^* \rightarrow \tau^+\tau^-$  and diboson production. The  $e^+e^-$  analysis uses a cut on sphericity  $\mathcal{S} = 3(\epsilon_1 + \epsilon_2)/2 > 0.15$ , where  $\epsilon_1$  and  $\epsilon_2$  are the two leading eigenvalues of the normalized momentum tensor [10]. This requirement rejects events in which jets are produced in a planar geometry through gluon radiation typical of background processes. The final selection applied in the  $\mu^+\mu^-$  channel further rejects the  $Z/\gamma^* \rightarrow \mu^+\mu^-$  background. We compute for each  $\mu^+\mu^-$  event the  $\chi^2$  of a fit to the  $Z \rightarrow \mu^+\mu^-$  hypothesis given the measured muon momenta and known resolutions. Figure 1 shows the predicted and observed  $\chi^2$  distribution in  $\mu^+\mu^- + \geq 1$  jet events. Selecting events with  $\chi^2 > 2$  is more effective than selecting on the dimuon invariant mass for this channel.

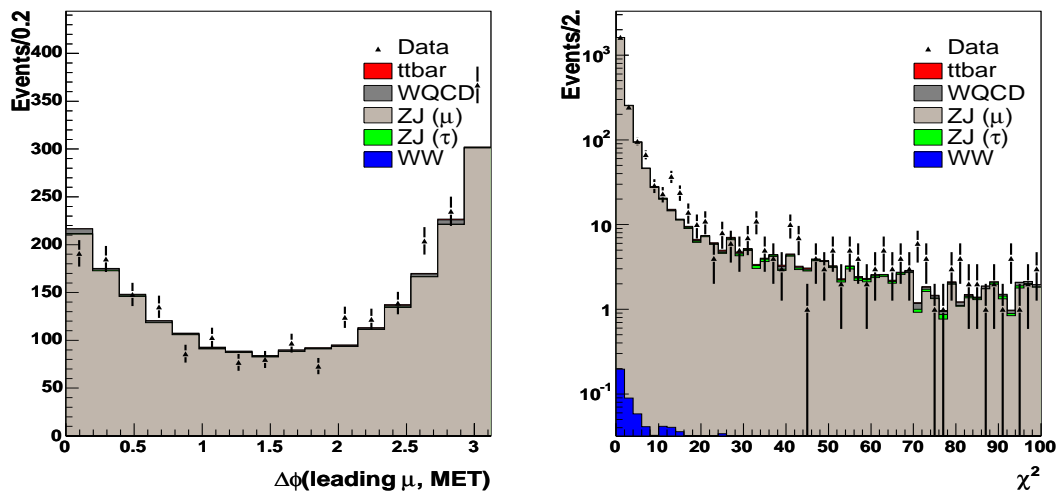


FIG. 1: Predicted and observed  $\Delta\phi$  between the  $\cancel{E}_T$  and the leading muon (left) and  $\chi^2$  (right) distribution for  $\mu^+\mu^- + \geq 1$  jet events.

### IV. SIGNAL EFFICIENCY

In order to compute the acceptances and efficiencies for the signal we generate  $t\bar{t}$  events at  $\sqrt{s} = 1.96$  TeV using the ALPGEN [11] matrix element generator assuming a top mass  $m_{top}$  of 175 GeV/ $c^2$ . These events are processed through PYTHIA [12] to provide fragmentation, hadronization and decays of short-lived particles. EVTGEN [13] is used to model the decays of  $b$  hadrons. The two  $W$ 's decay to two lepton-neutrino pairs, including all  $\tau$  final states. These events are processed through a full detector simulation using GEANT [14] providing tracking hits, calorimeter cell energy and muon hit information. Extra interactions are added to all events subject to Poisson statistics given the instantaneous luminosities typically observed in the run. The same reconstruction is applied to data and Monte Carlo events.

## V. BACKGROUND PROCESSES

Several background processes can fulfill the preselection criteria designed to select  $t\bar{t}$ . We distinguish two categories of backgrounds: “physics” and “instrumental”. Physics backgrounds are processes in which the charged leptons arise from electroweak boson decays and the  $\cancel{E}_T$  originates from high  $p_T$  neutrinos. This signature arises from  $Z/\gamma^* \rightarrow \tau^+\tau^-$  where the  $\tau$  leptons decay leptonically, and  $WW/WZ$  (diboson) production. Instrumental backgrounds are defined as events in which (a) a jet or a lepton within a jet fakes the isolated lepton signature, or (b) the  $\cancel{E}_T$  originates from misreconstructed jet or lepton energies or from noise in the calorimeter.

### A. Physics Backgrounds

The selection efficiencies for the physics backgrounds  $Z/\gamma^* \rightarrow \tau^+\tau^- \rightarrow \ell\ell'$  with  $\ell, \ell' = e$  or  $\mu$  and  $WW/WZ$  are estimated using Monte Carlo samples generated by ALPGEN followed by PYTHIA. The  $Z/\gamma^* \rightarrow \tau\tau$  process is normalized using the cross section measured by DØ [15]. For the diboson processes, diboson + 2 jets events are generated at leading order (LO) and are scaled by the ratio of the next-to-leading order to LO inclusive cross sections derived for diboson inclusive production [16]. The correction leads to an increase of 35% of the diboson prediction. A systematic uncertainty of 35% is also associated to the normalization of this background.

### B. Missing $E_T$ Instrumental Backgrounds

In the  $e^+e^-$  and  $\mu^+\mu^-$  channels the primary instrumental background arises from fake  $\cancel{E}_T$  in  $Z/\gamma^* \rightarrow ee, \mu\mu$  events. Detector resolutions can give rise to observed  $\cancel{E}_T$  imbalances in events which look like evidence of neutrinos. A contribution also arises from multijet production where both the lepton and the  $\cancel{E}_T$  are the result of mismeasurements rather than real high  $p_T$  charged leptons and neutrinos.

Once the jet, electron, muon and scalar  $E_T$  and jet resolutions of the Monte Carlo simulation have been adjusted to the measured resolutions in data, we observe in both the  $e^+e^-$  and the  $\mu^+\mu^-$  channels that the  $\cancel{E}_T$  spectrum observed in Monte Carlo agrees well with that in the data when selecting a pure sample of  $Z/\gamma^* \rightarrow ee, \mu\mu$  events in data. In the  $e^+e^-$  channel, we determine the probability that processes without real high  $p_T$  neutrinos pass the  $\cancel{E}_T$  selection from  $\gamma + 2$  jets candidate events. This sample is observed to have the same  $\cancel{E}_T$  distribution as  $Z/\gamma^* \rightarrow ee$  data and Monte Carlo. The probability to pass the  $\cancel{E}_T$  selection in the three samples is shown in Fig. 2. This probability is multiplied by the number of data events that fail the  $\cancel{E}_T$  selections but pass all other selections. In the  $\mu^+\mu^-$  channel, the expected contribution of  $Z/\gamma^* \rightarrow \mu^+\mu^-$  background in the final sample is derived directly from events simulated with ALPGEN. Good agreement is observed between the data and the simulation in the variables  $\cancel{E}_T$  and  $\Delta\phi(\cancel{E}_T, \mu_1)$ . This allows us to obtain the probability for a  $Z/\gamma^* \rightarrow \mu^+\mu^-$  event to pass the  $\cancel{E}_T$  selection from the simulation. The sample is normalized to the number of observed  $Z/\gamma^* \rightarrow \mu^+\mu^-$  events in the data with  $70 \leq M_{\mu\mu} \leq 110$  GeV before the  $\cancel{E}_T$  selection.

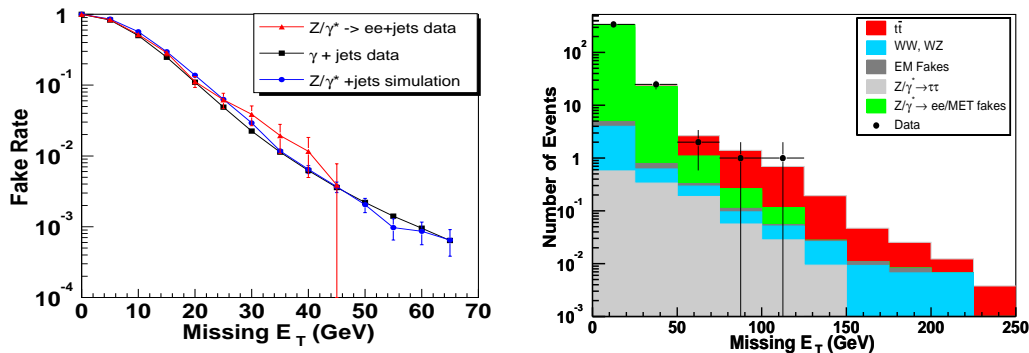


FIG. 2: Left: probability to pass the  $\cancel{E}_T$  selection as in the  $e^+e^-$  channel for events with 2 or more jets in  $Z/\gamma^* \rightarrow e^+e^-$  data events, in  $\gamma + 2$  jets data and for  $Z/\gamma^* \rightarrow e^+e^-$  Monte Carlo after object resolutions have been adjusted to data. Right: predicted and observed  $\cancel{E}_T$  spectrum in events with 2 electrons and 2 jets.

### C. Lepton Instrumental Backgrounds

Fake electrons can arise from instrumental effects. Jets comprised essentially of a leading  $\pi^0/\eta$  and an overlapping or conversion-produced track can for example mimic an isolated high  $p_T$  electron. In the  $e^+e^-$  channel we estimate this background by calculating the fraction  $f_e$  of loose electrons which pass the tight electron criteria in a control sample dominated by fake electrons. The control sample consists of events that satisfied the trigger and have two loose electrons. Contributions from processes with real electrons ( $W \rightarrow e\nu$  and  $Z/\gamma^* \rightarrow e^+e^-$ ) are suppressed by requiring  $\cancel{E}_T < 10$  GeV and  $|M_{ee} - M_Z| > 15$  GeV. We also veto events in which both electron candidates have a matching track. The predicted number of events with a fake electron in the final sample is obtained by multiplying the number of  $e^+e^-$  events with one loose electron and one tight electron by the fraction  $f_e$ .

In the  $e^\pm\mu^\mp$  channel a different approach is used. The electron is not required to be selected by the electron likelihood discriminant. Instead, the amount of fake electron background is fitted to the observed distribution of electron likelihood in data. To this end we first determine the shape of the electron likelihood for real electrons on a pure  $Z/\gamma^* \rightarrow ee$  sample. The shape of the electron likelihood for the fake electron background is determined in a sample dominated by fake electrons and selected in the following way. The muon is required to be anti-isolated instead of isolated (both calorimeter and tracker isolation greater than 20%) and  $\cancel{E}_T < 15$  GeV. The number of fake electrons in the selected sample is obtained by performing an extended likelihood fit to the observed distribution of electron likelihood in data. The likelihood is given by:

$$\mathcal{L} = \prod_{i=1}^N (n_e S(x_i) + n_{fake} B(x_i)) \frac{e^{-(n_e + n_{fake})}}{N!},$$

where  $i$  is an index that runs over all selected events,  $x_i$  is the corresponding observed value of the electron likelihood,  $N$  is the total number of selected events,  $n_e$  is the number of events with an isolated electron,  $n_{fake}$  is the number of events with a fake electron,  $S$  is the signal probability distribution function determined using real electrons and  $B$  is the background probability distribution function derived from the sample dominated by fake electrons. Figure 3 shows the shapes of the electron likelihood discriminant distributions in the real and fake electron samples and the distribution observed in data.

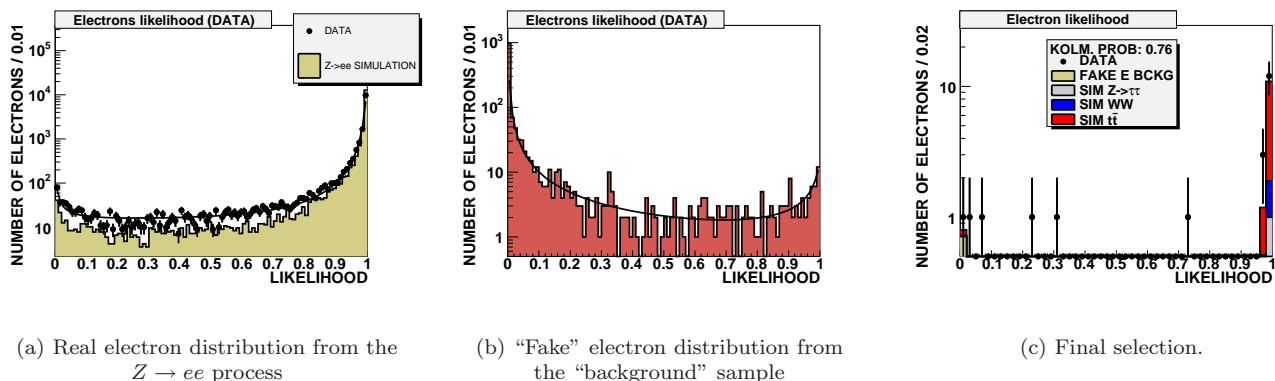


FIG. 3: Electron likelihood distributions.

An isolated muon can be mimicked by a muon in a jet when the jet is not reconstructed. We measure the fraction  $f_\mu$  of loose muons that satisfy the tight muon criteria in a control sample dominated by fake muons. In the  $\mu^+\mu^-$  channel the control sample is defined as events that have two loose muons. To suppress physics processes with real isolated muons the leading  $p_T$  muon is required to fail the tight muon criteria. This cuts efficiently  $Z/\gamma^* \rightarrow \mu^+\mu^-$  events but also  $W \rightarrow \mu\nu$  events where a second-leading muon might arise from a muon in a jet. The number of events with a fake muon contributing to the final sample is estimated by counting the number of events with one tight muon and a loose muon and multiplying it by  $f_\mu$ . In the  $e^\pm\mu^\mp$  channel the contribution from events where both leptons are fake leptons is already accounted for by using  $f_e$ . The remaining contribution from events with a real electron and a fake muon, is found to be negligible after extracting a muon fake rate  $f_\mu$  from data and applying it to simulated  $W \rightarrow e\nu$  events.

## VI. PREDICTION AND OBSERVATION

In Table I we summarize the predicted and observed number of events. The prediction for  $Z/\gamma^*$ , instrumental leptons and diboson backgrounds are also provided. Predicted and observed distributions for various event variables are shown in Fig. 5 and 4. Table V shows a display from a candidate event in the electron-muon channel.

Category	$ee$	$\mu\mu$	$e\mu$	$ll$
Integrated luminosity ( $\text{pb}^{-1}$ )	384	363	368	—
$Z/\gamma^*$	$0.75^{+0.18}_{-0.21}$	$1.01^{+0.22}_{-0.34}$	$1.22^{+0.33}_{-0.39}$	$2.98^{+0.43}_{-0.55}$
$WW/WZ$	$0.20^{+0.10}_{-0.14}$	$0.20^{+0.08}_{-0.07}$	$1.13^{+0.45}_{-0.48}$	$1.53^{+0.47}_{-0.50}$
Instrumental leptons	$0.09 \pm 0.03$	$0.13 \pm 0.04$	$2.13^{+2.50}_{-1.66}$	$2.35^{+2.50}_{-1.67}$
<b>Total background</b>	$1.0^{+0.2}_{-0.3}$	$1.3^{+0.3}_{-0.4}$	$4.5^{+2.6}_{-1.8}$	$6.8^{+2.6}_{-1.8}$
Signal efficiency	<b>0.082</b>	<b>0.064</b>	<b>0.139</b>	—
Expected signal	<b><math>3.5 \pm 0.4</math></b>	<b><math>2.5 \pm 0.3</math></b>	<b><math>11.3^{+1.2}_{-1.4}</math></b>	<b><math>17.3^{+1.3}_{-1.5}</math></b>
<b>SM expectation</b>	<b><math>4.5^{+0.4}_{-0.5}</math></b>	<b><math>3.8^{+0.4}_{-0.5}</math></b>	<b><math>15.8^{+2.8}_{-2.3}</math></b>	<b><math>24.1^{+2.9}_{-2.4}</math></b>
<b>Selected events</b>	<b>5</b>	<b>2</b>	<b>21</b>	<b>28</b>

TABLE I: Expected background and observed and expected signal yields. The expected signal yield is derived assuming  $\sigma_{t\bar{t}}=7$  pb. The errors on the yields are the quadratic sum of the statistical and the systematic errors.

## VII. RESULTS

The  $t\bar{t}$  cross section is measured by maximizing the product of the likelihoods for each individual channel based on the Poisson probability to observe a given number of events under the signal-plus-background hypothesis.

The preliminary  $t\bar{t}$  production cross sections at  $\sqrt{s}=1.96$  TeV in dilepton channels are measured to be:

$$\begin{aligned}
 ee : \quad \sigma_{t\bar{t}} &= 7.9^{+5.2}_{-3.8} \text{ (stat)} \quad {}^{+1.3}_{-1.0} \text{ (syst)} \pm 0.5 \text{ (lumi) pb} \\
 e\mu : \quad \sigma_{t\bar{t}} &= 10.2^{+3.1}_{-2.6} \text{ (stat)} \quad {}^{+1.6}_{-1.3} \text{ (syst)} \pm 0.7 \text{ (lumi) pb} \\
 \mu\mu : \quad \sigma_{t\bar{t}} &= 1.8^{+4.8}_{-3.0} \text{ (stat)} \quad {}^{+1.0}_{-1.2} \text{ (syst)} \pm 0.1 \text{ (lumi) pb} \\
 \text{dilepton} : \quad \sigma_{t\bar{t}} &= 8.6^{+2.3}_{-2.0} \text{ (stat)} \quad {}^{+1.2}_{-1.0} \text{ (syst)} \pm 0.6 \text{ (lumi) pb.}
 \end{aligned}$$

in good agreement with the standard model prediction of  $6.77 \pm 0.42$  pb [17].

The systematic uncertainty on the cross section measurement is obtained by varying the background and efficiencies, within their errors, with all the correlations between the channels and between the different classes of background taken into account. The dominant systematic uncertainties are summarized in Table II. Systematics uncertainties on the signal efficiencies and background expectations in each channel are shown in Tables III and IV. The following main systematics have been studied.

- **Jet energy calibration:** The measured jet energies in the calorimeter are corrected for the response of the calorimeter, showering outside the jet cone and energy from underlying activity in the event [9]. The uncertainty on the jet energy calibration is propagated to the predicted background yields and the efficiency for the  $t\bar{t}$  signal.
- **Lepton identification:** The lepton identification efficiencies are measured in data using well understood processes. They are studied in various detector regions, and various jet environments. Residual deviations from unity of the ratio of data to Monte Carlo efficiencies are used as systematic uncertainties.
- **Jet reconstruction and jet resolution:** Jet reconstructions and resolutions are determined in data and applied to Monte Carlo. Uncertainties on these data-derived quantities due to limited sample statistics and uncertainties related to the methods are propagated to signal and background predictions.

- **Fake electron background in the  $e\mu$  channel:** In the electron channel the shape of the electron likelihood discriminant is used to fit the number of fake electrons in the selected final sample. The shape itself is found to be depend on the electron  $p_T$  and the detector occupancy (number of jets). The number of fake electron is refitted with the various shapes to extract this systematic uncertainty on the background.
- **Trigger efficiency:** Trigger efficiencies are derived in data. They have uncertainties due to limited sample statistics. Various sources of bias are investigated, the resulting variations in trigger efficiencies are used as systematic error.

TABLE II: Summary of systematic uncertainties on  $\sigma_{t\bar{t}}$ .

Source	$\Delta\sigma_{t\bar{t}}$ (pb)
Jet energy calibration	+ 0.5 - 0.5
Jet identification	+ 0.5 - 0.4
Muon identification	+ 0.5 - 0.4
Electron identification	+ 0.4 - 0.3
Trigger	+ 0.7 - 0.4
Other	+ 0.4 - 0.4
Total	+ 1.2 - 1.0

Source	$ee$	$e\mu$	$\mu\mu$
Primary vertex	$\pm 0.4$	$\pm 0.4$	$\pm 0.4$
Electron reconstruction	$\pm 6.2$	$\pm 3.0$	N/A
Electron tracking and likelihood	$\pm 4.2$	N/A	N/A
Electron track match	N/A	$\pm 0.7$	N/A
Electron likelihood fit	N/A	+3.0 -4.0	N/A
Electron resolution	-0.9	N/A	N/A
Level 1 electron trigger	+1.2 -5.3	+0.1 -3.4	N/A
Level 3 electron trigger	$\pm 0.8$	+0.4 -0.5	N/A
$\mu$ identification	N/A	$\pm 4.0$	$\pm 8.0$
$\mu$ isolation	N/A	N/A	$\pm 0.8$
$\mu$ DCA significance	N/A	$\pm 0.5$	$\pm 0.6$
$\mu$ tracking	N/A	$\pm 3.0$	$\pm 2.5$
$\mu$ track $\chi^2$	N/A	$\pm 1.5$	$\pm 0.2$
$\mu$ resolution	N/A	N/A	-0.9
Level 1 $\mu$ trigger	N/A	+3.5 -4.4	$\pm 3.0$
Level 2 $\mu$ trigger	N/A	+3.6 -5.4	$\pm 0.1$
Opposite sign leptons	N/A	+2.0 -0.0	N/A
Jet energy calibration	+3.1 -5.0	+4.1 -4.0	+4.3 -4.4
Jet reconstruction	+4.2 -3.3	+2.7 -3.5	+6.0
Jet energy resolution	+1.8	+1.6 -3.8	+3.0

TABLE III: Summary of the relative systematic uncertainties on the  $t\bar{t} \rightarrow \ell\bar{\ell}$  signal efficiencies.

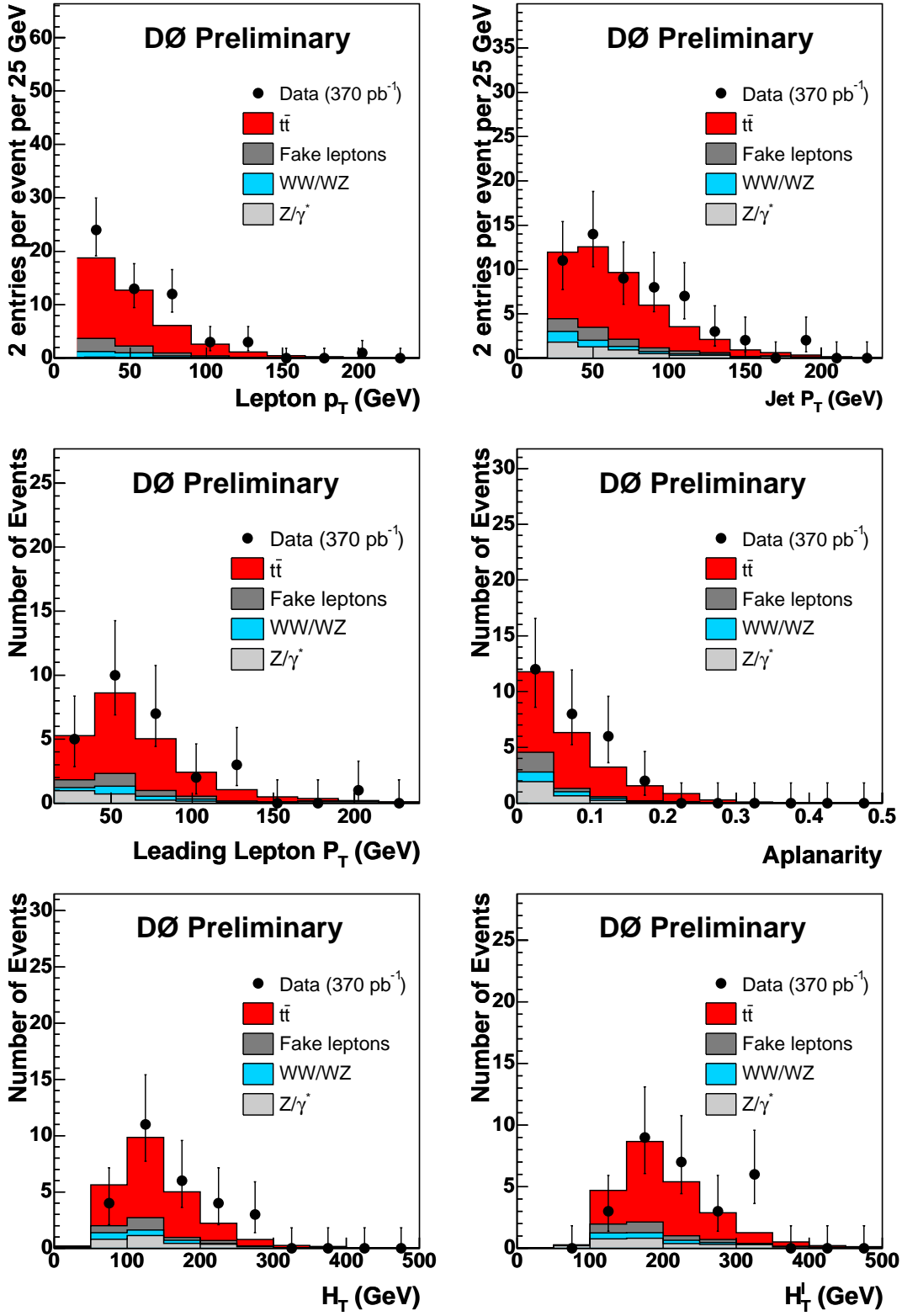


FIG. 4: Observed and predicted distributions for the various backgrounds and the signal. From top to bottom, lepton  $p_T$ , jet  $p_T$ , leading lepton  $p_T$ , aplanarity, scalar sum of jet  $p_T$  ( $H_T$ ) and scalar sum of jet  $p_T$  and leading lepton  $p_T$  ( $H_T^l$ ).

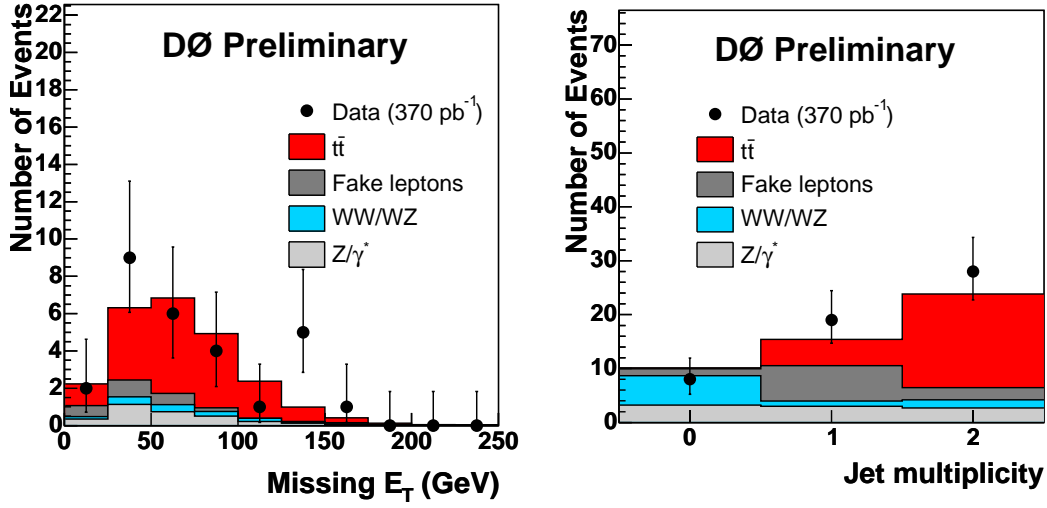


FIG. 5: Left: observed and predicted  $\cancel{E}_T$  distributions for the various backgrounds and the signal. Right: observed and predicted number of events with 0, 1 and 2 or more jets.

channel	$ee$		$e\mu$		$\mu\mu$	
	$WW$	$Z \rightarrow \tau\tau$	$WW$	$Z \rightarrow \tau\tau$	$WW$	$Z/\gamma^*(\mu \text{ or } \tau)$
Source						
Primary vertex	$\pm 0.4$	$\pm 0.4$	$\pm 0.4$	$\pm 0.4$	$\pm 0.4$	N/A
Electron reconstruction	$\pm 6.4$	$\pm 6.7$	$\pm 3.0$	$\pm 3.0$	N/A	N/A
Electron tracking and likelihood	$\pm 3.6$	$\pm 3.7$	N/A	N/A	N/A	N/A
Electron track match	N/A	N/A	$\pm 0.7$	$\pm 0.7$	N/A	N/A
Level 1 electron trigger	+1.4 -6.4	+2.7 -16	+0.2 -14	+0.1 -13	N/A	N/A
Level 3 electron trigger	$\pm 1.1$	$\pm 4.1$	+0.4 -0.5	+1.0 -1.1	N/A	N/A
$\mu$ identification	N/A	N/A	$\pm 4.0$	$\pm 4.0$	$\pm 8.0$	N/A
$\mu$ isolation	N/A	N/A	N/A	N/A	$\pm 0.8$	N/A
$\mu \sigma_{dca}$	N/A	N/A	$\pm 0.5$	$\pm 0.5$	$\pm 0.6$	N/A
$\mu$ tracking	N/A	N/A	$\pm 3.0$	$\pm 3.0$	$\pm 2.5$	N/A
$\mu$ track $\chi^2$	N/A	N/A	$\pm 1.5$	$\pm 1.5$	$\pm 0.2$	N/A
$\mu$ resolution	N/A	N/A	N/A	N/A	+0.3 -2.2	+1.2 -18
Level 1 $\mu$ trigger	N/A	N/A	+3.9 -4.8	+3.6 -4.4	+3.7 -3.6	+11
Level 2 $\mu$ trigger	N/A	N/A	+3.7 -5.6	+3.6 -5.6	+0.2 -0.1	+11
Opposite sign leptons	N/A	N/A	+2.0 -0.0	+2.0 -0.0	N/A	N/A
Jet energy calibration	+7 -10	+16 -22	+14 -13	+16 -18	+8 -24	+26 -3
Jet reconstruction	-37	-25	+6 -7	+7 -8	-45	N/A
Jet energy resolution	-30	+8 -6	$\pm 3.2$	$\pm 7$	-17	+16
Normalization	$\pm 35$	$\pm 7$	$\pm 35$	$\pm 9$	$\pm 35$	$\pm 7$

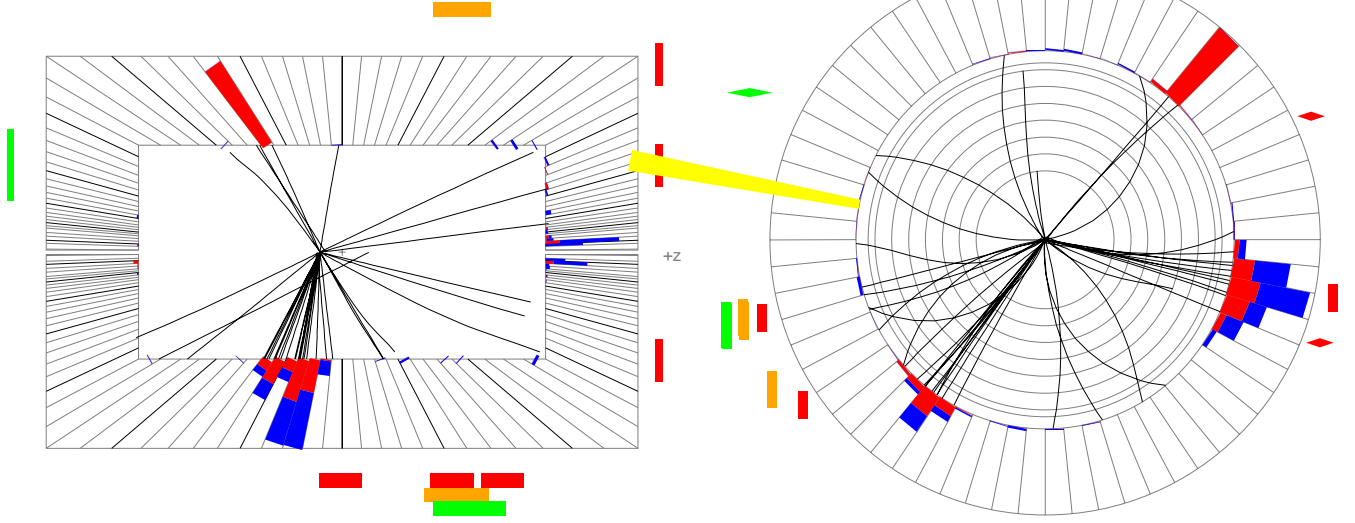
TABLE IV: Summary of the relative systematic uncertainties on background.

Run 193332 Evt 3472458 Tue Jan 25 15:58:40 2005

Run 193332 Evt 3472458 Tue Jan 25 15:58:40 2005

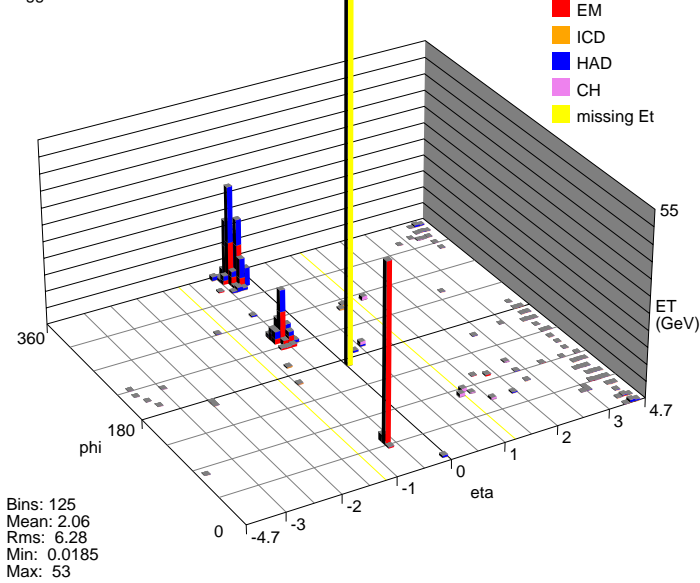
E scale: 63 GeV

ET scale: 54 GeV



Run 193332 Evt 3472458 Tue Jan 25 15:58:40 2005

Triggers:



Object	$p_T$ (GeV)	$\eta$	$\phi$	likelihood
electron	65.097	-0.539	0.853	0.969
muon	48.148	0.565	3.400	
jet 1	192.272	-0.183	6.027	
jet 2	80.943	-0.425	4.080	
$\cancel{E}_T$	156.022		2.630	

mE\_t: 147  
 phi\_t: 169 deg

One

TABLE V:  $e - \mu$  candidate event: Run Number:193332, Event Number: 3472458. The table in the lower right corner shows basic kinematic quantities for jets and leptons in the event.

### VIII. ACKNOWLEDGMENTS

We thank the staffs at Fermilab and collaborating institutions, and acknowledge support from the DOE and NSF (USA); CEA and CNRS/IN2P3 (France); FASI, Rosatom and RFBR (Russia); CAPES, CNPq, FAPERJ,

FAPESP and FUNDUNESP (Brazil); DAE and DST (India); Colciencias (Colombia); CONACyT (Mexico); KRF (Korea); CONICET and UBACyT (Argentina); FOM (The Netherlands); PPARC (United Kingdom); MSMT (Czech Republic); CRC Program, CFI, NSERC and WestGrid Project (Canada); BMBF and DFG (Germany); SFI (Ireland); Research Corporation, Alexander von Humboldt Foundation, and the Marie Curie Program.

- 
- [1] J.F. Gunion *et al.*, *The Higgs Hunters Guide* (Addison-Wesley, Redwood City, California, 1990), p. 200.
- [2] S. Eidelman *et al.*, Phys. Lett. B **592**, 1 (2004).
- [3] CDF Collaboration, D. Acosta *et al.*, Phys. Rev. Lett. **93**, 142001 (2004); DØ Collaboration, V. Abazov *et al.*, FERMILAB-PUB-05-217-E, hep-ex/0505082.
- [4] DØ Collaboration, V. Abazov *et al.*, “The Upgraded DØ Detector,” in preparation for submission to Nucl. Instrum. Meth. Phys. Res. A.
- [5] Rapidity  $y$  and pseudo-rapidity  $\eta$  are defined as functions of the polar angle  $\theta$  and parameter  $\beta$  as  $y(\theta, \beta) \equiv \frac{1}{2} \ln [(1 + \beta \cos \theta)/(1 - \beta \cos \theta)]$ ;  $\eta(\theta) \equiv y(\theta, 1)$ , where  $\beta$  is the ratio of a particle’s momentum to its energy.
- [6] DØ Collaboration, S. Abachi *et al.*, Nucl. Instrum. Methods Phys. Res. A **338**, 185 (1994).
- [7] V. Abazov *et al.*, FERMILAB-PUB-05-034-E (2005)
- [8] Jets are defined using the iterative seed-based cone algorithm with  $\Delta\mathcal{R} = \sqrt{(\Delta\phi)^2 + (\Delta\eta)^2} = 0.5$  (where  $\phi$  is the azimuthal angle), including mid-points as described in Sec. 3.5 (p. 47) of G. C. Blazey *et al.*, in *Proceedings of the Workshop: “QCD and Weak Boson Physics in Run II,”* edited by U. Baur, R. K. Ellis, and D. Zeppenfeld, FERMILAB-PUB-00-297 (2000).
- [9] DØ Collaboration, B. Abbott *et al.*, Nucl. Instrum. Meth. A **424**, 352 (1999).
- [10] V. Barger, J. Ohnemus, and R. J. N. Phillips, Phys. Rev. D **48**, 3953 (1993).
- [11] ALPGEN, M.L. Mangano *et al.*, JHEP 0307:001, 2003, hep-ph/0206293.
- [12] PYTHIA, Physics and Manual, T. Sjöstrand *et al.*, LU TP 01-21, hep-ph/0108264.
- [13] D. J. Lange, Nucl. Instrum. Methods Phys. Res. A **462**, 152 (2001).
- [14] R. Brun and F. Carminati, CERN Program Library Long Writeup W5013, 1993 (unpublished).
- [15] DØ Collaboration, V. Abazov *et al.*, Phys. Rev. D **71**, 072004 (2005).
- [16] J. M. Campbell and R. K. Ellis, Phys. Rev. D **60**, 113006 (1999).
- [17] R. Bonciani *et al.*, Nucl. Phys. **B529**, 424 (1998); N. Kidonakis and R. Vogt, Phys. Rev. D **68**, 114014 (2003); M. Cacciari *et al.*, JHEP **404**, 68 (2004).